Stripping properties of a plasma medium for MeV/u chlorine ions

M. Chabot,[1] D. Gardès,[1] P. Box,[1] and J. Kiener,[1] C. Deutsch,[2] G. Maynard,[2] V. André,[3] C. Fleurier,[3] D. Hong,[3] and K. Wohrer[4]

[1]*Institut de Physique, Nucléaire, Orsay IN2P3, France*

[2]*Laboratoire de Physique des Gaz et des Plasmas, Orsay, France*

[3]*Groupe de Recherche sur l'Energétique et la Matière Ionisée, Orléans, France*

[4]*Groupe de Physique des Solides, Paris VII, France*

(Received 14 October 1994)

Clear experimental evidence of plasma stripping enhancement for 1.5 MeV/u chlorine ions is contrasted with its cold gas homologue at the same density (1×10^{19} e^-/cm^{-2}). The plasma is created by an electrical discharge in hydrogen and diagnosed with optical spectroscopic methods and beam probe analysis. The velocity dependence for the charge distributions is modeled both in cold gas and in plasma experiments. The calculations are found to be in good agreement with the hypothesis of a strongly reduced capture rate in the plasma case. Those results document quantitatively the basic mechanisms underlying the enhanced ion projectile charge in a plasma target. They also add credence to currently advocated scenarios for heavy-ion-driven fusion.

PACS number(s): 41.75.Ak, 52.40.Mj, 52.20.Hv, 34.70.+e

I. INTRODUCTION

Stripping properties of solid and gaseous media have been extensively studied for many years, either for application in heavy-ion accelerators or for basic physical issues [1,2]. Implementation of plasma targets on accelerator beam lines [3,4] creates an opportunity to investigate the stripping properties of this new medium.

When a swift heavy ion penetrates a solid or gaseous medium it exchanges energy in collisions with bound electrons. During this process successive electron captures and losses occur, leading to an equilibrium charge state. In a plasma medium, electrons are free and the capture probability of free electrons depends on recombination processes associated with very low cross sections such as radiative transfer or dielectronic recombination [5,6]. As a result, an ion penetrating a plasma should increase rapidly its charge state up to a value larger than the cold matter equilibrium charge.

This paper presents experimental evidence for such effects. The choice of the chlorine ion at 1.5 MeV/u was determined by a compromise between the ability to perform a complete theoretical treatment of the evolution of the charge-state distribution (high velocity and low atomic number) and, on the other hand, by the possibility for this particular collision to produce a significant difference between the plasma and cold-gas target, which is expected to increase at low velocity and with a high-Z projectile.

In the first part, the experimental setup is described and special attention is paid to the plasma characteristics. In a second part, a modeling that numerically solves a set of rate equations for the different final charge states is compared to the experimental results for charge-state distributions in cold gas and plasma.

II. EXPERIMENTAL SETUP

Chlorine beams were delivered by the Orsay MP Tandem Van de Graaff accelerator. The incident energy was defined with an energy resolution $\Delta E/E = 10^{-4}$. The diameter of the beam was 3 mm during its travel through the plasma tube. The negative ion source of the machine was run in a pulsed mode in order to reach high instantaneous intensities without destroying the stability of the voltage machine. The beam was then transported through a 90° analyzing magnet and a stripper device, which allowed for the selection of a given charge state at the target entrance.

A. Cold-gas target

A quartz tube (52 cm long and 0.5 cm in diameter) was filled with hydrogen or deuterium gas, cycled with a continuous flow. The tube was enclosed between two fast valves [7] that were opened only during measurement. The flow rate was regulated with a mass flow controller (accuracy ±0.8%). The pressure was controlled through an absolute pressure gauge (baratron) with a 0.5% accuracy. In those experiments the pressure ranged from 10^{-2} torr up to 10 torr. The beam arrival was synchronized with the tube unlocking. A laser beam transmission measurement showed that a time of 200±5 μs was required for a full opening of the plasma tube by means of the fast valves. Therefore, the beam pulse had to be injected 200 μs after the start of the opening. During this short time the leakage flux through the collimators toward the beam line was measured and found to be 2.5% of the starting pressure. Under secondary pumping, the composition of the residual gas (2.10^{-3} torr) inside the

tube was analyzed by means of a mass spectrometer and found to consist essentially of water molecules.

B. Plasma target

1. Design features

We essentially made use of the same dense discharge as that already used previously [4,5]. For the plasma target, the same quartz tube filled with hydrogen or deuterium was fired, using an electrical discharge through the gas. The current profile is given as

$$I = I_0 \sin(\omega t) e^{-t/\tau} ,$$

with $I_0 = 6$ kA; $\omega = 2\pi/2.5\times10^{-5}$ s^{-1} and $\tau = 22.5\times10^{-6}$ s. Discharge current and gas ejection through tube apertures constrain the electron density to change rapidly with time. After a few microseconds the gas gets completely ionized, which yields a plasma with a linear density of the order of $1\times10^{19} e^-/cm^2$. The complete exploration of the density range has been performed by synchronizing and tuning the arrival time of a short ion-beam burst during the plasma time evolution.

2. Plasma diagnostics

The density and temperature of the plasma were measured using methods already presented elsewhere [8] that are essentially based on Stark line broadening, laser absorption at two different wavelengths, and laser interferometry. All diagnostic measurements were performed along the tube axis, which is also the beam axis. Therefore, they could only be performed off line in the absence of the beam.

During on-line operations, the plasma was monitored through the transverse light emission. From corresponding measurements, stability and reproducibility of the plasma were derived. The density was diagnosed via thermodynamics and line-broadening models. This control is subject to a larger uncertainty than in the longitudinal determination, due to the small thickness of the plasma in this transverse direction and to a density gradient near the tube's wall.

Spectroscopic and optical methods are not very sensitive in detecting very small contamination rates of (heavy) impurities. However, such a contamination can strongly affect the evolution of the charge distribution of the chlorine ions relative to situations in pure plasma or cold gas. For this purpose, an ion beam was used as a probe to investigate both heavy element impurities and proton density. The method is detailed in Refs. [9] and [10]. The principle of the measurement is based on charge-exchange and ionization processes on a hydrogen-like chlorine ion beam (Cl^{16+}) at 4.3 MeV/u. For this particular beam, it is found that the main contributions for electron capture and ionization come from the heavy contaminants and the protons, respectively. With these conditions, measurements on Cl^{15+} heliumlike ion production and Cl^{17+} bare ion production provide, respectively, access to the heavy element and proton densities inside the plasma target. A good agreement was found with the optical diagnostic presented previously for the proton density and was compatible with the residual pressure (2×10^{-3} torr) measurement for the heavy elements' contamination. Figure 1 presents the electron linear density as a function of time.

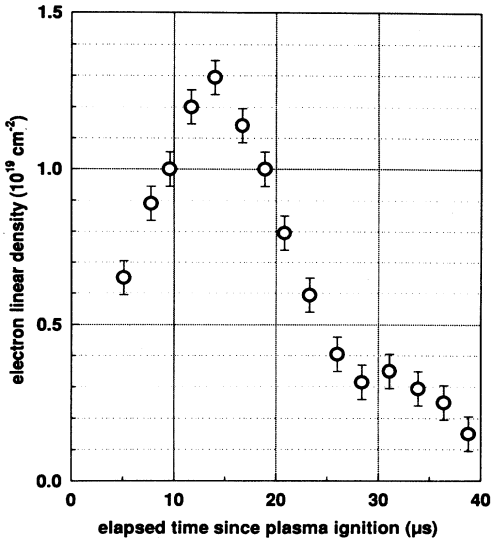

FIG. 1. Plasma density as a function of time.

C. Magnetic spectrometer and detection system

After interaction with the target, the beam was magnetically analyzed. A slit in front of a magnetic spectrometer defined the entrance trajectories. The position of the ion impact after deflection by the magnetic field was detected by a plastic scintillator (NE102A, 1 mm thick), viewed by a fast camera that produces intensified images on a charge coupled device (CCD). The CCD output is connected to a digital computer interface.

D. Data analysis

The background of the CCD noise was subtracted for each image. Afterwards, the images were projected along the dispersive direction. The resulting charge distributions were fitted by convolution of Gaussian distributions using the PAW software library from CERN [11]. The area under each peak profile was proportional to the number of detected ions of a specific charge state. An example of a charge-state distribution is given in Fig. 2.

E. Perturbation due to plasma lens effects

A specific feature of the linear discharge arises from the generation of an intense azimuthal magnetic field varying linearly from a zero value on the axis to a maximum value on the outer radius r:

$$B = \mu_0 j r/2 ,$$

where j is the current density and r the radius of the column. The beam interacting with the plasma column is collinear with the current direction (Fig. 3). Depending on the relative directions of the current and of the beam,

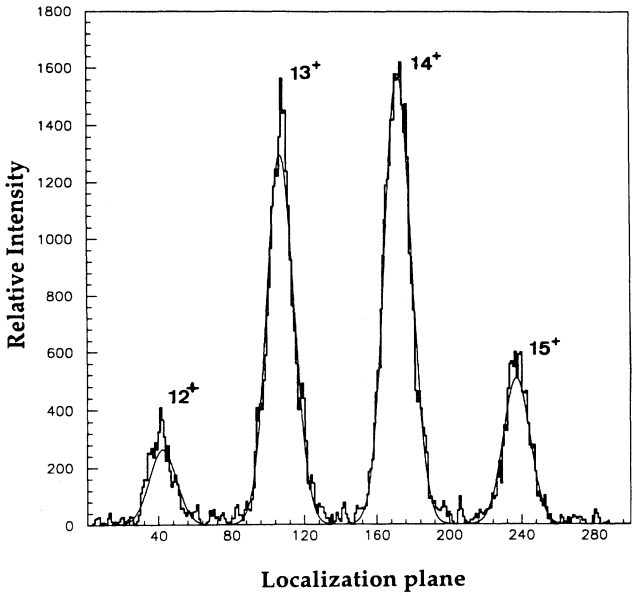

FIG. 2. Charge-state distribution for Cl ions obtained on the plastic scintillator. The histogram corresponds to the data and the solid line to the Gaussian fit.

the Lorentz force may have a strong radial component and will tend to focus or defocus the ion beam. Such a property of the linear plasma discharge has been extensively studied to generate efficient plasma lenses [12,13]. In the case of charge-state measurements, this effect is a real nuisance, because for a given value of the current, the focal length F is a function of the beam charge state

$$F=[\sqrt{k}\sin(\sqrt{k}\,l)]^{-1},$$

with

$$k=\frac{q}{p}\mu_0\times\frac{j}{2},$$

where l is the plasma length, p the ion momentum, and q the charge state of the ion.

As a consequence, the beam size at the entrance slits of the magnetic spectrometer depends on the charge state. Figure 3 illustrates this dependence on the transmitted intensity through the magnet slit. To evaluate quantitatively this effect, a Monte Carlo computer code has been developed in which the initial velocity of individual ions was confined to a realistic phase-space emittance figure. A correction factor has been obtained for the transmission through the slit of the different charge states. In the worst case, this factor reached 50% when there was a relative abundance of the observed charge states.

In any case, a treatment of this plasma lens distortion must include the "charge history" during the ion travel through the plasma. This evolution is a key issue in the study. In order to overcome this problem, the results reported here are limited to the events that correspond to measurements independent of that effect, that is to say, when the beam is strongly defocused for all charge states arriving on the slits. In this particular case, the transmission ratio defined by the slit aperture is identical for all the components of the charge-state distribution.

III. RESULTS AND DISCUSSION

A. Cold-gas measurements

1. Experimental charge-state distributions

The evolution of the charge-state distributions as a function of the gas pressure was measured for two incident charge states of the projectile: 13^+ and 15^+ and a beam energy of 1.5 MeV/u. Experimental results are presented in Figs. 4 and 5. Entering with a 13^+ or 15^+, the chlorine ion reaches an equilibrium charge state equal to 13.18 ± 0.02. These values are in agreement with equilibrium charge-state determination in hydrogen obtained previously [14]. Solid curves pertain to the model calculation detailed in the Sec. III A 2.

2. Model calculation for cold gas

The final charge distributions of chlorine ions traversing various target thicknesses are obtained by solving the complete set of linear differential coupled equations governing capture and ionization rates. Double charge-exchange processes have been neglected and each of these

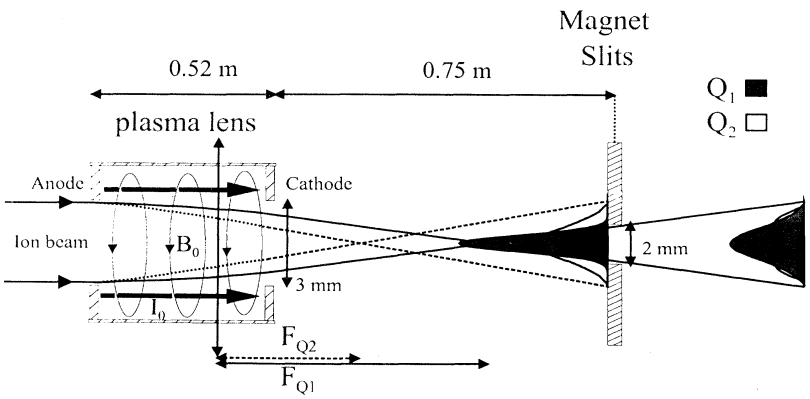

FIG. 3. Plasma lens effect and its influence on the charge-state distribution. The relative intensity passing through the slit depends on the focusing distance, i.e., on the charge state of the ion.

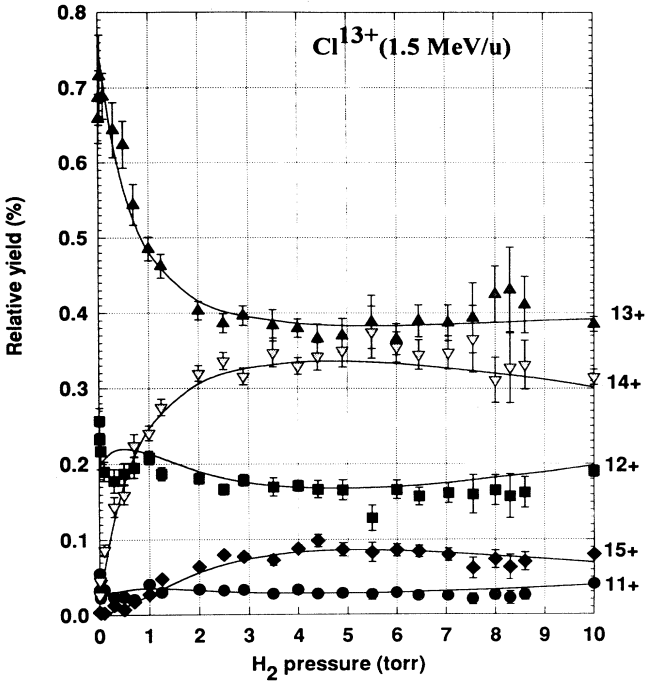

FIG. 4. Charge state evolution in cold gas. Cl^{13+} incident ion.

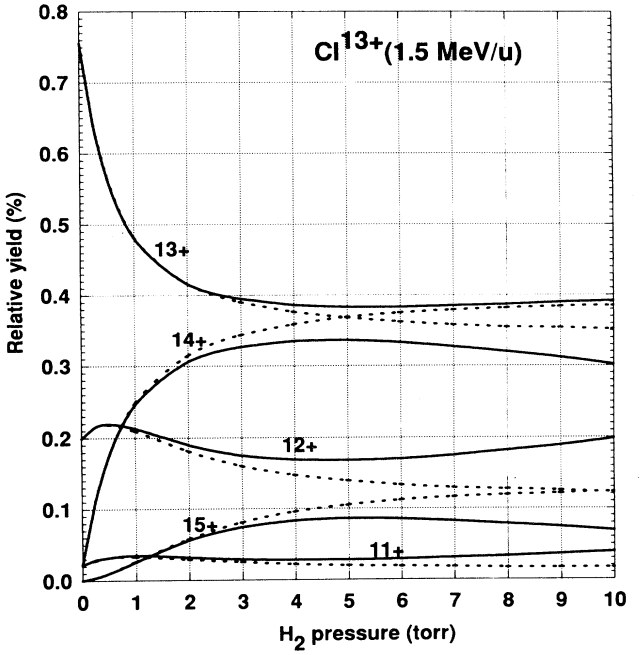

FIG. 6. Velocity dependence of cold-gas charge-state distributions. Dotted curves correspond to the constant velocity approximation.

rate equations couples a given charge state q to the two closest neighbor charge states $q+1$ and $q-1$. The low density of the target (some 10^{17} H/cm^3) allows us to consider that the ions, which are excited after each collision, do have enough time to relax to their ground state before the next interaction has taken place. Metastable states have also been neglected. Therefore, cross sections that are inserted in this calculation refer to ground-state configurations. Contributions from heavy impurities are also included in the model.

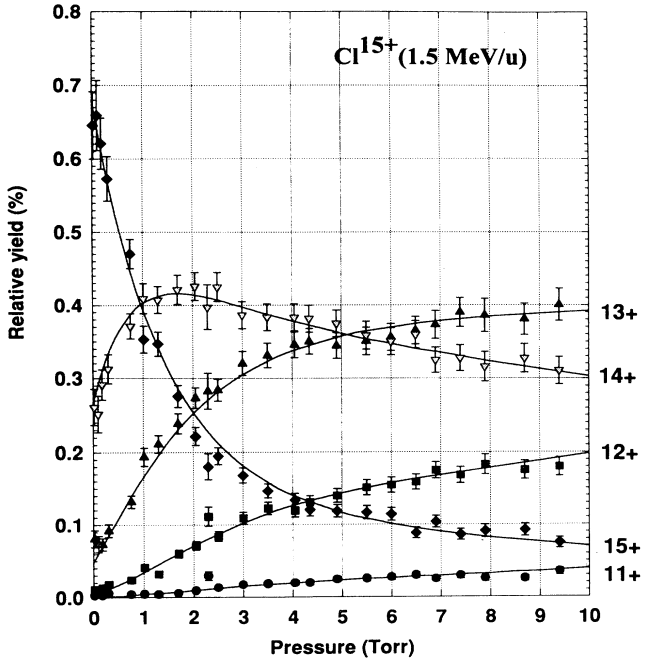

FIG. 5. Charge state evolution in cold gas. Cl^{15+} incident ion.

The cross sections for heavy impurities are deduced from measurements in residual gas, while the cross sections for hydrogen gas are adjusted to fit the experimental evolution of the charge-state distribution with the target density for both incident Cl^{13+} (Fig. 4), and Cl^{15+} (Fig. 5) ion beams. The strong velocity dependence of capture cross sections associated with the deceleration process of the chlorine ions during their travel through the gas cell has been fully taken into account. The results of this calculation presented in Fig. 6, together with the constant velocity approximation, show that the velocity effect must be included at high pressure measurements.

3. *Comparison with experimental results*

Capture and ionization cross sections corresponding to the best fit of the cold-gas charge-state distributions are displayed in Tables I and II together with theoretical calculations and empirical predictions from Refs. [15–21]. The plane wave Born approximation (PWBA) has been applied to the proton ionization cross section [15,16]. Dependence on the projectile configuration uses effective charge derived from Ref. [17]. The value of the proton ionization cross section (corrected PWBA) has been improved by introducing several corrections proposed by Brandt [18], who takes into account the Coulomb deflection of the ion trajectory and a molecular effect in the vicinity of the hydrogen target atom at low velocities. At higher velocities a polarization term that corresponds

TABLE I. Ionization cross sections. Values are in cm^2.

Ion	Last e^- configuration	PWBA proton	Corrected PWBA	Free electron	Bound electron	Sum proton + electron	Sum used in computer code	Total for all electrons	Total used in computer code
Cl^{16+}	$1s$	7.53×10^{-22}	5.44×10^{-22}	0	2.54×10^{-27}	5.44×10^{-22}	1.07×10^{-21}	5.44×10^{-22}	1.07×10^{-21} [a]
Cl^{15+}	$1s^2$	9.85×10^{-22}	7.29×10^{-22}	0	4.00×10^{-27}	7.29×10^{-22}	1.34×10^{-21}	1.46×10^{-21}	2.67×10^{-21} [a]
Cl^{14+}	$1s^2$	1.08×10^{-21}	8.10×10^{-22}	0	4.74×10^{-27}	8.10×10^{-22}	1.34×10^{-21}		
Cl^{14+}	$2s$	6.67×10^{-20}	6.26×10^{-20}	6.77×10^{-22}	3.86×10^{-21}	6.49×10^{-20}	5.04×10^{-20}	6.65×10^{-20}	5.31×10^{-20}
Cl^{13+}	$1s^2$	1.18×10^{-21}	8.89×10^{-22}	0	5.54×10^{-27}	8.89×10^{-22}	1.34×10^{-21}		
Cl^{13+}	$2s^2$	7.59×10^{-20}	7.15×10^{-20}	7.02×10^{-21}	7.90×10^{-21}	7.90×10^{-20}	7.38×10^{-20}	1.60×10^{-19}	1.50×10^{-19}
Cl^{12+}	$1s^2$	1.32×10^{-21}	1.01×10^{-21}	0	6.87×10^{-27}	1.01×10^{-21}	1.34×10^{-21}		
Cl^{12+}	$2s^2$	8.61×10^{-20}	8.14×10^{-20}	1.40×10^{-20}	1.36×10^{-20}	9.52×10^{-20}	7.38×10^{-20}		
Cl^{12+}	$2p$	9.69×10^{-20}	9.51×10^{-20}	2.47×10^{-20}	2.35×10^{-20}	1.19×10^{-19}	1.67×10^{-19}	3.11×10^{-19}	3.17×10^{-19}
Cl^{11+}	$1s^2$	1.45×10^{-21}	1.13×10^{-21}	0	8.31×10^{-27}	1.13×10^{-21}	1.34×10^{-21}		
Cl^{11+}	$2s^2$	1.01×10^{-19}	9.56×10^{-20}	2.39×10^{-20}	2.29×10^{-20}	1.19×10^{-19}	7.38×10^{-20}		
Cl^{11+}	$2p^2$	1.16×10^{-19}	1.14×10^{-19}	3.89×10^{-20}	3.71×10^{-20}	1.52×10^{-19}	2.59×10^{-19}	5.44×10^{-19}	6.69×10^{-19}
Cl^{10+}	$1s^2$	1.61×10^{-21}	1.27×10^{-21}	0	1.03×10^{-26}	1.27×10^{-21}	1.34×10^{-21}		
Cl^{10+}	$2s^2$	1.17×10^{-19}	1.12×10^{-19}	3.50×10^{-20}	3.38×10^{-20}	1.46×10^{-19}	7.38×10^{-20}		
Cl^{10+}	$2p^3$	1.40×10^{-19}	1.38×10^{-19}	5.65×10^{-20}	5.45×10^{-20}	1.94×10^{-19}	2.79×10^{-19}	8.77×10^{-19}	9.84×10^{-19} [a]

[a]This cross section plays a minor role in the charge-state distribution.

to the second order term in the Born approximation is added to the theory. Screening effects due to the hydrogen electrons have been computed with a Thomas-Fermi approximation and are found to be negligible. Ionization cross sections by free electrons are calculated by using the Moores formalism [19], and bound-electron ionization is estimated in the sudden impulse approximation. In this latter case, the electron ionization cross section is integrated over the full hydrogen momentum distribution.

Table I presents the total ionization cross sections associated with each charge state. The computed cross sections are compared with total ionization cross sections used in the code (last column). The values result from the contribution of all the electronic shell components to the ionization process. The agreement is remarkable and always remains within a 30% discrepancy. Capture cross sections resulting from the fit are compared to predictions in Table II of Schlachter *et al.* [20] and Nakaï [21] and are found to lie within the confidence range given by these authors.

TABLE II. Capture cross sections. Values are in cm^2.

Ion	Slachter	Nakaï	Model values
Cl^{17+}	3.51×10^{-19}	3.24×10^{-19}	2.43×10^{-19} [a]
Cl^{16+}	2.78×10^{-19}	2.72×10^{-19}	2.07×10^{-19} [a]
Cl^{15+}	2.17×10^{-19}	2.27×10^{-19}	1.70×10^{-19}
Cl^{14+}	1.66×10^{-19}	1.86×10^{-19}	1.40×10^{-19}
Cl^{13+}	1.25×10^{-19}	1.51×10^{-19}	1.13×10^{-19}
Cl^{12+}	9.16×10^{-20}	1.20×10^{-19}	9.00×10^{-20}
Cl^{11+}	6.54×10^{-20}	9.36×10^{-20}	4.20×10^{-20} [a]
Cl^{10+}	4.53×10^{-20}	7.13×10^{-20}	3.96×10^{-20} [a]

[a]This cross section plays a minor role in the charge-state distribution.

B. Plasma measurements

1. Experimental results

For the two incident charge states 13^+ and 15^+, the final charge-state distributions after interaction with fully ionized hydrogen are compared in Figs. 7 and 8 to the corresponding cold-gas distributions. This comparison has been performed during the optimum transmission

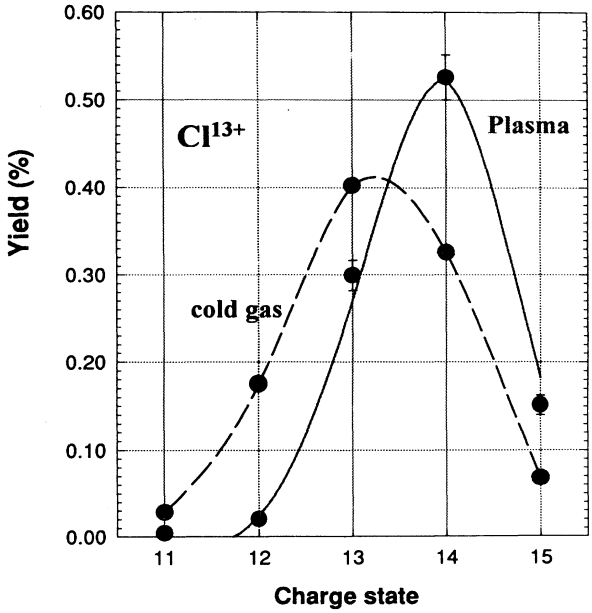

FIG. 7. Comparison between cold-gas and plasma charge-state distribution. Cl^{13+} incident ion. The lines represent the model calculation for cold gas (dashed line) and plasma (solid line).

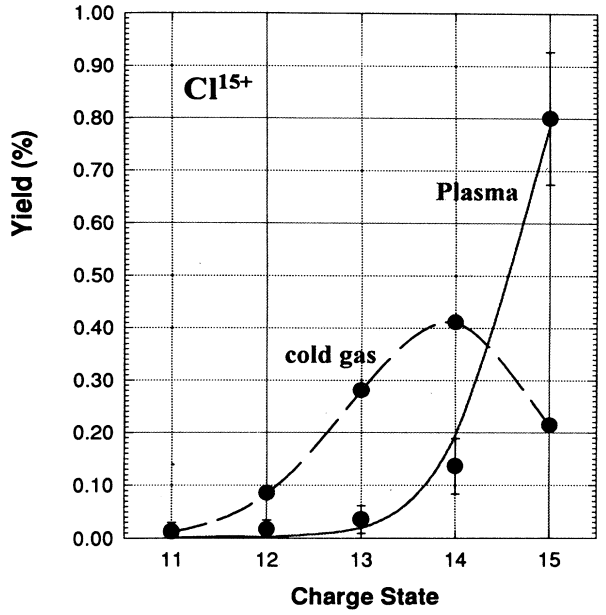

FIG. 8. Comparison between cold-gas and plasma charge-state distribution. Cl^{15+} incident ion. The lines represent the model calculation for cold gas (dashed line) and plasma (solid line).

period (see Sec. II E). At that moment the linear density of the target was $(1.0\pm0.1)\times10^{19}e^{-}/cm^2$ and the ionization degree was $95\pm5\%$. The enhancement of the stripping efficiency of the plasma medium shows up clearly with the 13^+ incident projectile. The mean charge state is displaced from 13.18 up to 13.87 in the plasma case. For the 15^+ incident charge (Fig. 8), a frozen charge-state effect is observed, in agreement with channeling experiments [22,23]. The error bars that are reported on the graphs reflect experimental uncertainties on peak localization, Gaussian fitting, and remaining plasma lens effects.

2. *Plasma calculation*

The calculation in the plasma case is based on the following three assumptions:

(i) The capture cross section of free electrons is zero. This approximation is justified considering that the cross sections associated with radiative charge transfer are roughly three orders of magnitude lower than the bound-electron capture cross sections. Moreover, dielectronic recombination processes are determined by resonant features that need not be considered in this particular velocity range [24].

(ii) The ionization cross section for the free electron-proton pair is taken to be half the ionization cross section for the hydrogen molecule. That is to say that the proton is not screened by the bound electron and that ionization by bound or free electrons is equal.

(iii) The cross sections on the impurities are the same in the cold gas and in the plasma medium.

The plasma temperature (2 eV) is not high enough to ionize more than one outer shell electron of heavy impurities. This electron makes only a small contribution to the total charge transfer cross section [25] and its role in the screening remains negligible for the ionization process.

3. *Comparison with the model*

In Figs. 7 and 8 are reported the calculated distributions (full curves) corresponding to the above assumptions. Within the experimental error bars, the agreement between experimental and computed charge-state distributions is remarkable and supports the validity of this simple modeling. The theoretical cross sections presented in Table II are well established; thus the agreement between cross sections used to fit the experimental data and the calculated values for both a cold and hot target tends to show that the basic physical issues corresponding to the plasma are included in such a phenomenological model.

C. Discussion

The influence of the plasma on the charge evolution is illustrated in Fig. 9. Using the atomic cross sections of Tables I and II, we present the atomic rates for ionization τ_i and for the capture of one electron τ_e in terms of the projectile charge state for both cold gas and the plasma target:

$$\tau_i=(n_e\sigma_i^{\mathrm{H}}+n_i\sigma_i^I)V\ ,$$

$$\tau_c=(n_H\sigma_c^{\mathrm{H}}+n_i\sigma_c^I)V\ ,$$

where n_e, n_i, and n_{H} are the electron (bound and free), impurity, and atomic hydrogen densities. $\sigma_{i,c}^{\mathrm{H}}$ and $\sigma_{i,c}^I$ are the atomic cross sections for collisions with atomic

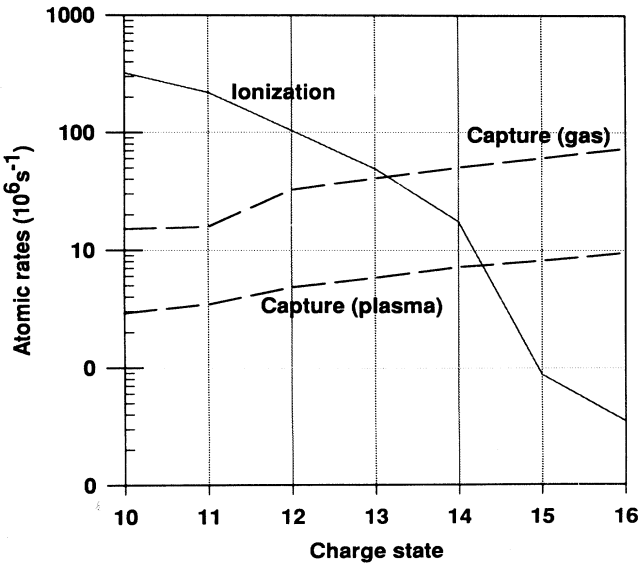

FIG. 9. Ionization and one electron capture rates versus the projectile charge state for Cl^{q+} at 1.5 MeV/u in gas and plasma target, respectively.

hydrogen and impurities. V is the projectile velocity.

Figure 9 clearly demonstrates the charge changing behavior due to the plasma target: an unchanged ionization and a strongly reduced capture. In the plasma case the residual capture arises only from the remaining neutral hydrogen (some percent of the total density) and also from the heavy impurities. The crossing between the ionization and the capture curves correspond to the equilibrium charge values. In the gas case, we retrieve the experimental value of 13.2.

In the general case of ion interaction with matter, three media can be distinguished for charge changing:

(i) The cold-gas medium where all the ionization and capture processes are effective.

(ii) The free electron medium, like that in channeling experiments, where the main capture and ionization processes are suppressed (no more ionization by nuclei).

(iii) The plasma medium where capture is reduced, like in channeling experiments, but where ionization on nuclei remains significant.

As a consequence, the plasma target appears as the most effective stripping medium for heavy ion beams in the MeV/u velocity range.

IV. CONCLUSION

This paper presents clear experimental evidence of the plasma stripping enhancement of the ion projectiles. For the chlorine ions that are considered in this article, the difference between cold gas and plasma increases with a decreasing beam velocity. At 2 MeV/u and with a plasma density of 1×10^{19} cm^{-2}, this effect remains negligible [9]. At 1.5 MeV/u and at the same plasma density, the charge-state distribution of Cl^{13+} incident ions is shifted toward higher values than in the corresponding cold-gas medium. This velocity dependence, but also the complexity of the plasma apparatus and the timing constraint, limit the ability of such a process in accelerator applications. On the other hand, this behavior is of great interest for the study of inertial confinement fusion driven by heavy ions, because the stopping process is largely determined by the dynamically controlled evolution of the charge state of the projectile.

Further experiments are necessary to investigate more accurately the correlation between the projectile charge-state evolution and the corresponding stopping power amplitude and straggling in the plasma target.

[1] G. D. Alton, R. A. Sparrow, and R. E. Olson, Phys. Rev. A **45**, 5957 (1992).

[2] E. Nardi and Z. Zinamon, Phys. Rev. Lett. **49**, 1251 (1982).

[3] D. H. H. Hoffmann, K. Weyrich, H. Wahl, D. Gardès, R. Bimbot, and C. Fleurier, Phys. Rev. A **42**, 2313 (1990).

[4] D. Gardès, A. Servajean, B. Kubica, C. Fleurier, D. Hong, C. Deutsch, and G. Maynard, Phys. Rev. A **46**, 5101 (1992).

[5] G. Maynard, W. André, M. Chabot, C. Deutsch, C. Fleurier, D. Gardès, D. Hong, K. Kiener, M. Pouey, and K. Wohrer, Nuovo Cimento **106**, 1825 (1994).

[6] T. Peter and J. Meyer-ter-Vehn, Phys. Rev. A **43**, 2015 (1991).

[7] C. Fleurier, J. Mathias, B. Dumax, J. Pellicer, A. Bonnet, D. Gardès, and B. Kubica, Nucl. Instrum. Methods Phys. Res. B **61**, 236 (1991).

[8] C. Fleurier, A. Sanba, D. Hong, J. Mathias, and J. C. Pellicer, J. Phys. C **7**, 141 (1988).

[9] M. Chabot, D. Gardès, J. Kiener, S. Damache, B. Kubica, C. Deutsch, G. Maynard, M. Pouey, W. André, C. Fleurier, D. Hong, and K. Wohrer, Nuovo Cimento A **106**, 1789 (1993).

[10] M. Chabot *et al.*, in *Laser and Particle Beams,* edited by George Miley (Cambridge University, Cambridge, in press).

[11] Physics Analysis Workstation (PAW), Computing and Networks Division, CERN, Geneva, Switzerland.

[12] E. Boggasch, J. Jacoby, H. Wahl, K. G. Dietrich, D. H. H. Hoffmann, W. Laux, M. Elfers, C. R. Haas, V. P. Dubenkov, and A. A. Golubev, Phys. Rev. Lett. **66**, 1705 (1991).

[13] A. Tauschwitz, E. Boggasch, D. H. H. Hoffmann, M. de Magistris, U. Neuner, M. Stetter, R. Tkotz, T. Wagner, W. Seelig, and H. Wetzler, Nuovo Cimento A **106**, 1733 (1993).

[14] R. Bimbot and M. F. Rivet (unpublished).

[15] G. S. Khandelwal, B. H. Choi, and E. Merzbacher, At. Data **1**, 103 (1969).

[16] B. H. Choi, E. Merzbacher, and G. S. Khandelwal, At. Data **5**, 291 (1973).

[17] R. Marchand, S. Caillée, and Y. T. Lee, J. Quant. Spectrosc. Radiat. Transfer **43**, 149 (1990).

[18] W. Brandt and G. Lapicki, Phys. Rev. A **20**, 465 (1979).

[19] D. L. Moores, L. P. Golden, and D. H. Sampson, J. Phys. B **134**, 385 (1980).

[20] A. S. Schlachter, J. W. Stearns, W. G. Graham, K. A. Berkner, R. V. Pyle, and J. A. Tanis, Phys. Rev. A **27**, 3372 (1983).

[21] Y. Nakaï, M. Shirai, T. Tabata, and R. Ito, At. Data Nucl. Data Tables **37**, 69 (1987).

[22] J. A. Golovchenko, A. N. Goland, J. S. Rosner, C. E. Thorn, H. E. Wegner, H. Knudsen, and C. D. Moak, Phys. Rev. B **23**, 957 (1981).

[23] S. Andriamonje, B. Blank, R. del Moral, J. P. Dufour, L. Faux, A. Fleury, M. S. Pravikoff, C. Röhl, M. Chevallier, D. Dauvergne, R. Kirsh, J. C. Poisat, J. Remilleux, C. Cohen, Y. Girard, A. L'Hoir, J. P. Rozet, D. Schmaus, D. Vernhet, J. Dural, H. Rothard, M. Toulemonde, Y. Quéré, and N. Cue, Nucl. Instrum. Methods Phys. Res. B **87**, 116 (1994).

[24] G. Maynard and C. Deutsch, Phys. Scr. **48**, 471 (1993).

[25] D. Z. Belkic, R. Gayet, and A. Salin, Phys. Rep. **6**, 279 (1979).

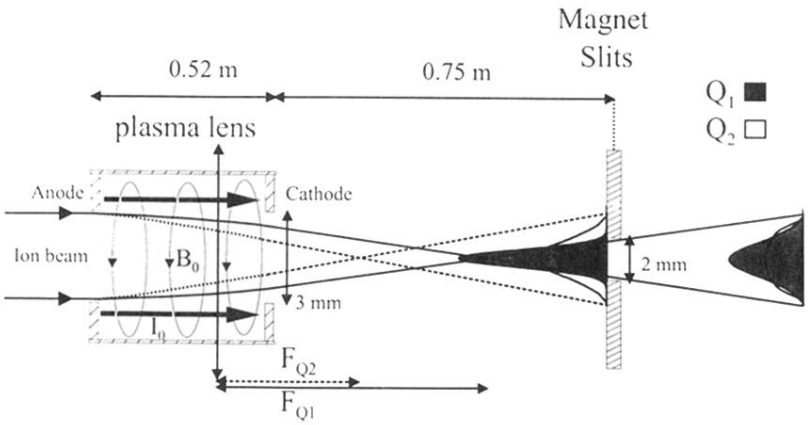

FIG. 3. Plasma lens effect and its influence on the charge-state distribution. The relative intensity passing through the slit depends on the focusing distance, i.e., on the charge state of the ion.